Crystalline Raman Lasers

James A. Piper and Helen M. Pask

(Invited Paper)

***Abstract*—In this paper, we review the developments of crystalline Raman lasers over the past five years. Average powers exceeding 5 W and pulse energies above 1 J in the near infrared have been demonstrated for larger scale devices. There has been a rapid development of all-solid-state sources based on the standard diode-pumped lasers, especially intracavity crystalline Raman lasers, which offer wavelength versatility at high conversion efficiencies (overall diode Stokes optical conversion efficiencies up to 17%) in the near infrared, including the 1.5-μm eye-safe band. Passively Q-switched intracavity Raman lasers based on self-Raman laser materials offer many advantages for miniaturization of short-pulse ($<$1 ns) sources. Intracavity frequency-doubled crystalline Raman lasers have also emerged as practical and versatile sources in the yellow orange region at $>$1-W power levels with diode-visible efficiencies near 10%. Recent developments of all-solid-state continuous-wave (CW) intracavity crystalline Raman lasers offer many possibilities for the future: intracavity frequency doubling has already resulted in the demonstration of CW visible sources with powers approaching 1 W at 5% diode-visible efficiency.**

***Index Terms*—All-solid-state Raman lasers, continuous wave (CW) Raman lasers, crystalline Raman lasers, stimulated Raman scattering (SRS).**

I. Introduction

THE PAST DECADE, and most particularly the past five years, has seen a rapid escalation in interest and associated number of reports on lasers and laser frequency conversion based on stimulated Raman scattering (SRS) in crystalline materials. Crystalline Raman lasers have generated both high average powers ($>$5 W) and high pulse energies ($>$1 J), with conversion efficiencies in some cases approaching the quantum limit, and output wavelengths spanning key spectral regions including the eye-safe near infrared and the green to red range of the visible, with significant progress in extension to the midinfrared and ultraviolet. Intracavity Raman lasers based on the standard diode-pumped solid-state laser materials, or utilizing a range of self-Raman laser materials, have the capability of generating a variety of new near infrared laser wavelengths with diode Stokes optical efficiencies approaching 20%. The inclusion of nonlinear second-harmonic generation (SHG) or sum-frequency generation (SFG) in intracavity devices has been shown to be an effective means for yellow red generation at diode-visible optical efficiencies approaching 10%. And while the great majority of Raman lasers up to the present time have operated in pulsed mode (picosecond to nanosecond), there has been dramatic progress in only the past two years in the development of continuous-wave (CW) Raman oscillators generating in the near infrared, and most recently in the yellow, by way of intracavity SHG of CW Raman lasers operating in the near infrared. Additionally, the variety of practical Raman crystals coupled with a choice of the fundamental (pump) laser medium permits an extensive range of wavelengths to be accessed with minimal variation in the basic laser configuration.

Also of great significance has been developments in semiconductor waveguide Raman lasers, including the first demonstrations of silicon Raman lasers [80], [81]. This work is not within the scope of the present review of crystalline Raman lasers, which is confined to bulk insulating crystalline materials.

SRS in bulk insulating crystalline materials (e.g., diamond, calcite) was first reported in 1963 [1], very soon after the discovery of the laser itself, but it was not until a decade later that the potential to use crystalline Raman materials for laser frequency conversion in a practical way was demonstrated. In particular, in the pioneering work by Ammann reported over the period 1975–1979 [2]–[4], optical efficiencies as high as 77% were obtained for intracavity Raman conversion in crystalline $LiIO_3$ (LI) from the 1064-nm fundamental of a Q-switched neodymium-doped yttrium aluminium garnet (Nd:YAG) laser to the first-Stokes Raman output at 1156 nm. Intracavity frequency doubling of the first-Stokes Raman field in the $LiIO_3$ itself, generated over 0.5 W of yellow (578 nm) output at fundamental-to-yellow optical conversion efficiencies of $\sim$20%. Shortly thereafter, Eremenko *et al.* [5] reported $>$25% efficiency for conversion of nanosecond 532-nm pulses to first-Stokes Raman output in crystalline $Ba(NO_3)_2$ (BN), an excellent Raman medium that has become the basis for many Raman devices reported subsequently. In parallel with the experimental SRS studies in this early period, the theory of SRS had also been well established, initially by Bloembergen in 1967 [6] and later by Kaiser and Maier [7], Wang [8], Penzkofer *et al.* [9], and others.

Given the platform for development of crystalline Raman lasers that existed by 1980, it is perhaps surprising that there appears to have been comparatively little interest over the next decade in the development of practical devices based on SRS in crystals. However, key results reported by Andryunas *et al.* [10] on self-Raman conversion in Nd:$KGd(WO_4)_2$ (Nd:KGW) and Nd:$KY(WO_4)_2$ (Nd:KYW) in the picosecond domain, Karpukhin and Stepanov [11] on external cavity BN (also, $NaNO_3$ and $CaCO_3$) Raman lasers operating in the nanosecond domain, and Basiev *et al.* [12] on efficient second-Stokes Raman shifting (in BN) to the 1.5-μm eye-safe spectra laid the foundation for the developments of the next decade.

Manuscript received November 8, 2006; revised March 21, 2007. This work was supported in part by the Australian Research Council, in part by the (Australian) Defence Science and Technology Organization, and in part by Macquarie University.

The authors are with Macquarie University, Sydney NSW 2109, Australia (e-mail: jim.piper@vc.mq.edu.au; hpask@ics.mq.edu.au).

Digital Object Identifier 10.1109/JSTQE.2007.897175

The reawakening of international interest in Raman laser development based on crystal materials was triggered by parallel (and sometimes joint) reports over the period 1993–1995 by Basiev [12], Zverev *et al*. [13], and Murray *et al*. [14] of eye-safe (1.53–1.56 μm) Raman lasers based on BN pumped by Nd^{3+} lasers in various resonator configurations. There followed a rapid expansion in the number of reports internationally of research on crystalline Raman lasers aimed at the development of practical devices for a wide range of applications, for example, remote sensing in defence and atmospheric science, biomedical diagnostics, and laser therapies (in dermatology and ophthalmology). The biomedical applications, in particular, have driven our own developments [15], [16] of all-solid-state yellow orange sources based on intracavity frequency-doubled crystalline (LI and KGW) Raman lasers themselves pumped intracavity by diode-pumped Nd:YAG or vanadate lasers.

The recent blossoming of research activity in crystalline Raman lasers is strongly underpinned by the key technical advances of the past decades: development and ready availability of new crystalline Raman materials (notably the tungstates) with high optical quality, and especially, high damage threshold; the parallel developments of high-power diode-pumped solid-state lasers; and understanding of the effects of thermal loading in the Raman crystal and how this needs to be dealt with in Raman resonators, especially intracavity Raman lasers where the combination of thermal loading in both the Raman and laser crystals poses particular challenges in resonator design. The attraction of self-Raman crystals (e.g., Nd:vanadates, tungstates, and molybdates) for miniaturization of devices has also been a significant factor recently.

The present paper builds on three major reviews of solid-state (crystalline) Raman lasers published some three to four years ago by Basiev and Powell [17], Pask [18], and Cerny *et al*. [19]. It does not seek to give a comprehensive review of research before 2002, since this is covered very well by the preceding reviews, but rather focuses on the developments of the past five years with the aim of establishing the state-of-the-art of solid-state Raman lasers at the time of publishing. We commence with short summaries of SRS theory, material properties of practically important Raman crystals, and recent results for single-pass Raman conversion of short-pulse lasers, and subsequently, focus on developments of Raman lasers in external resonators, intracavity lasers (including self-Raman lasers), intracavity frequency-doubled Raman lasers for visible generation, and finally, CW crystalline Raman lasers.

II. Phenomenon and Theory of SRS

Spontaneous Raman scattering involves inelastic scattering of light in an optical medium, which simultaneously deposits energy into an excited state of the component matter, the scattered photons having energy reduced by the quantum of energy deposited in the process. The scattered light accordingly has frequency $\omega_{S1} = \omega_P - \omega_R$, where ω_P is the frequency of the incident (or pump) light, and $\hbar\omega_R$ matches the energy of an electronic, vibrational, or rotational energy state of the Raman medium. In the case of the crystalline Raman media of interest here, $\hbar\omega_R$ matches a vibrational mode of the crystal. Where the energy of the scattered photon is less than that of the incident photon (as in the equality above), the scattered light has longer wavelength and is referred to as the (first) Stokes line.

SRS arises from the third-order nonlinear polarizability $P_3 = \varepsilon_0\chi_3 E^3$ of the optical medium (ε_0 is the dielectric constant, χ_3 is the third-order nonlinear susceptibility, and E is the amplitude of the incident optical field). Also, χ_3 gives rise to other common nonlinear phenomena including two-photon absorption, stimulated Brillouin scattering, and self-focusing. These effects, most importantly self-focusing, can sometimes compete with SRS as outlined in [18]. SRS relates to the imaginary part of χ_3 which is proportional to the *square* of the normal-mode derivative of the molecular polarizability tensor $\partial\alpha/\partial q$ [20] Materials with high polarizability and for which the vibrational modes modulate the polarizability strongly, as for symmetric breathing modes of covalently bound molecules, are favored for SRS [21], [22].

The theory of SRS has been the subject of several papers and texts [6]–[9], [20] and has been reviewed again by Basiev and Powell [17] and Pask [18]; thus, a review here is not intended. It is sufficient for current purposes to present the standard expression for growth along the propagation direction z of the intensity $I_s(z)$ of the Stokes field near the threshold (i.e., disregarding depletion of the incident/pump field I_p) in the *steady-state* regime

$$I_s(z) = I_s(0)\exp(g_R I_p z)$$

where the steady-state Raman gain coefficient is

$$g_R = \frac{8\pi c^2 N}{\hbar\mu_S^2\omega_S^3\Gamma}\left(\frac{\partial\sigma}{\partial\Omega}\right)$$

and the integrated Raman scattering cross section is introduced as

$$\frac{\partial\sigma}{\partial\Omega} = \frac{\omega_S^4\mu_S}{c^4\mu_P}\frac{\hbar}{2m\omega_R}\left(\frac{\partial\alpha}{\partial q}\right)^2.$$

Here, N is the number density of Raman-active molecules, μ_S and μ_P are the refractive indices at the Stokes and pump wavelengths, respectively, m is the reduced mass of the molecular oscillator, and Γ is the linewidth of the Raman transition, which is equal to the inverse of the dephasing time T_R for the final state of the transition ($\Gamma = T_R^{-1}$). The value of integrated Raman scattering cross section and the polarization of the Stokes-scattered light depend on the orientation of the crystal, and thus, the relevant vibrational mode, with respect to the polarization of the incident (pump) light. Approximations in the theory preclude generation of Stokes light with polarization orthogonal to that of the pump, and although this is not strictly true, for most practical purposes, the strongest Stokes scattering (and therefore, the gain) is obtained for Stokes polarization parallel to the pump polarization.

The *steady-state* regime applies when the incident pump pulse duration τ_P is long compared with the dephasing time T_R, which for most molecules of interest here is $\sim$10 ps (28 ps for BN [17]). It follows that for pump pulses anywhere longer than $\sim$1 ns, the steady-state formulas apply. Examination of these shows that the steady-state Raman gain coefficient g_R is higher for shorter Stokes wavelength (i.e., larger ω_s), larger integrated scattering cross section (i.e., larger $\partial\alpha/\partial q$), and smaller Raman linewidth

TABLE I
KEY SPECTRAL PROPERTIES FOR SELECTED RAMAN CRYSTALS [17]–[19], [26], [27], [32]

Crystal (abbrev)	Raman shift cm^{-1}	Raman linewidth cm^{-1}	Integrated cross-sec (arb units*)	Raman gain g_L @1064nm cm/GW	Raman gain g_L @532nm cm/GW	Damage threshold GW/cm^2
$LiIO_3$ (LI)	822	5.0	54	4.8		~ 0.1
$PbMO_4$ (PM)	870	8	~50	~8		~ 0.4
$Sr MO_4$ (PM)	888	2.8	55	~6		
$Ba(NO_3)_2$ (BN)	1047	0.4	21	11	47	~ 0.4
$BaWO_4$ (BW)	926	1.6	52	8.5	40	
$CaWO_4$ (CW)	908	4.8	52	3.0		~ 0.5
$KGd(WO_4)_2$ (KGW)	768 901	6.4 5.4	59 54	4.4 3.5	11.8	~ 10
$KY(WO_4)_2$ (KYW)	767 905	8.4 7	65 50	3.6 5.1	21	
$PbWO_4$ (PW)	904	4.7		3.1		~1
$SrWO_4$ (SW)	922	2.7	50	5.0		~ 5
$GdVO_4$ (GV)	885	3.0	92	>4.5		~ 1
YVO_4 (YV)	892	2.6	92	>4.5		~ 1

* Units for integrated Raman scattering cross section are normalized to 100 by comparison to diamond.

$\Delta\omega_R$ (i.e., smaller $\Gamma = 2\pi c\Delta\omega_R$). We shall see later that BN has only a moderate integrated Raman scattering cross section, but a very narrow Raman linewidth (0.4 cm^{-1}), which leads to a high steady-state Raman gain $\sim$11 cm/GW at 1.06 μm.

In the absence of an injected Stokes signal, SRS grows from the spontaneous Stokes noise I_{SN}, integrated over the line width ΔW_R of the Raman transition and scattered into solid angle $\Delta\Omega$ given by $I_S(0) = \frac{\hbar\omega_S^3\mu_S^3}{(2\pi)^3c^2}\Delta\Omega$. Since this typically has a value $\sim 10^{-15}$ W/cm^2, in order to reach Raman "threshold" (usually defined as 1% depletion of the pump), the exponent $g_R I_P z$ generally needs to have a value of 30 or more. For a crystal with steady-state gain coefficient $g_R \sim 10$ cm/GW (e.g., BN) and length 30 mm, this requires that the pump intensity I_P to reach the threshold exceeds 1 GW/cm^2, a value which is above the damage threshold of many candidate Raman crystals.

The *transient* Raman regime applies when the incident/pump pulse duration τ_P is much shorter than the dephasing time T_R. Here, the Stokes signal grows as

$$I_s(z) = I_{SN}\exp\left(-\frac{\tau_P}{T_R}\right)\exp\left[2\left(\frac{\tau_P g_R I_P z}{T_R}\right)^{1/2}\right].$$

Since g_R depends on Γ^{-1} and $\Gamma T_R = 1$, we see that in the transient regime, Stokes growth is independent of Raman linewidth, and the exponent depends on $z^{1/2}$ rather than on z as for the steady-state case. Thus, Raman crystals with high-integrated Raman scattering cross section are preferred for the transient regime. Note also that the growth exponent depends on the *energy* $\tau_P I_P$ of the pump pulse rather than the intensity, and the overall gain drops rapidly as τ_P becomes much less than T_R due to the first exponential term.

In either the steady-state or transient SRS regimes, where the intensity (or energy) of the (first) Stokes-shifted line (frequency ω_{S1}) becomes large, the threshold for SRS of the first-Stokes line itself may be exceeded, and the so-called second-Stokes line (frequency $\omega_{S2} = \omega_{S1} - \omega_R$) is then generated. Likewise, the third-Stokes line ($\omega_{S3} = \omega_{S2} - \omega_R$) may be generated from the second-Stokes, and so on. The phenomenon of multiple-Stokes generation is fairly common in the cases of short-pulse pumping with very high intensities (in either steady-state or transient regime), and in the steady-state regime, where the Raman crystal is placed within a resonator, which has high-Q (low-loss) for the lower order Stokes lines (say, the first- and second-Stokes) but has high coupling losses for the next higher order Stokes line (say, the third-Stokes). We see later how this can be used effectively in external cavity and intracavity Raman lasers to generate wavelength-versatile lasers in which particular output wavelengths can be selectably generated with high optical conversion efficiency.

III. PROPERTIES OF CRYSTALLINE RAMAN MEDIA

A. Raman and Related Optical Properties

There have been extensive programs of growth and analysis of crystalline materials for application to Raman frequency conversion of lasers over the past three decades, especially in the laboratories of the General Physics Institute and the Institute of Crystallography, Russian Academy of Science. Summaries of properties of crystal materials relevant to SRS are given in a number of articles including the Basiev and Powell review [17] and related earlier articles [23], [24], and articles by Kaminskii *et al*. [25]–[27].

Crystals fulfilling the requirements for high polarizability are the covalently bound iodates, nitrates, tungstates, and molybdates. There are many possible variations of these: those that have emerged in the literature as showing both good SRS performance and the potential for practical implementation are listed in Table I. Given our earlier estimate that the threshold for single-pass Raman generation requires incident intensities $\sim$1 GW/cm^2, susceptibility of prospective Raman crystals to optical damage is an important factor in materials selection as well as availability of quality crystals of large size. We note that, for

TABLE II
RELEVANT THERMAL PROPERTIES OF SELECTED RAMAN CRYSTALS [17], [18], [33]

	$LiIO_3$	$CaWO_4$	$Ba(NO_3)_2$	$KGd(WO_4)_2$	YVO_4	$BaWO_4$
thermal conductivity k_c at 25°C $Wm^{-1}K^{-1}$		16	1.17	2.5-3.4	5.2	3.0
thermal expansion α mK^{-1} ($x10^{-6}$)		6.35||a 12.38||c	13	1.6-8.5	4.4	6
thermo-optic coeff dn/dT K^{-1} ($x10^{-6}$)	-85 (o) -69 (e)	-7.1 (o) -10.2 (e)	-20	-0.8 (p[gg]p) -5.5 (p[mm]p)	3	

example, although high optical conversion efficiencies and average powers have been reported by several authors [2]–[4], [28] for first-Stokes generation in the near infrared in lithium iodate, use of LI in practical devices is compromised by its low optical damage threshold ($\sim$100 MW/cm^2 for nanosecond pulses). Likewise, barium nitrate (BN) has the highest Raman gain of those crystals listed, but is hygroscopic and has only moderate optical damage threshold ($\sim$0.4 GW/cm^2 for nanosecond pulses); so, it must be treated with care in practical situations. Calcium tungstate is also susceptible to mechanical and optical damage.

The availability of quality crystals of the harder tungstates over the past few years has been a key factor in the growing interest in Raman lasers. KGW has a high-integrated Raman scattering cross section, which favors its use for transient SRS, a comparatively broad Raman linewidth, which lowers the steady-state Raman gain, but most importantly, a very high damage threshold (KYW has similar optical properties). Evaluation of barium tungstate (BW), undertaken only some six years ago, showed this crystal to have very desirable optical characteristics for SRS such as: high Raman cross section and narrow Raman linewidth, resulting in both high steady-state Raman gain and excellent performance in the picosecond-pulse regime as well as optical damage threshold approaching to that of KGW [29], [30]. Strontium and lead tungstates (SW, PW) also exhibit desirable properties for SRS but they both suffer somewhat by comparison to BW. The molybdates have high scattering cross sections and narrow Raman linewidths, but they also appear to have lower optical damage thresholds [31]. The vanadates $GdVO_4$ and YVO_4 (GV, YV) are very common laser host materials, which have been ignored as Raman materials until quite recently [27], but which have excellent optical properties for SRS in the steady-state regime.

Comparisons of BN, KGW, and BW for SRS in the steady-state regime (nanosecond pump pulses at 1.06 μm) show that Raman thresholds for effectively identical experimental conditions are ordered as BN lowest to KGW highest, though fundamental to first-Stokes slope efficiencies are similar [30]. Subsequent studies of SRS in SW under similar conditions [17] demonstrated Raman threshold intermediate between BW and KGW. More recent studies of SRS in the vanadate crystals GV and YV in the steady-state regime show the Raman gain is similar to that of KGW and KYW, though the scattering cross sections estimated from spectral data suggest the steady-state gain should be about double as that for KGW [32]. We note finally that in the choice of Raman crystal for SRS of short pulses $\tau_P \sim 10-40$ ps, the dephasing time T_R is an important consideration since it governs the transition from the steady-state to the transient regime, where the gain is substantially reduced.

B. Thermal and Thermooptic Properties

Although the Raman and related optical properties of crystals are a good guide to how different crystal media will perform in SRS under pulsed pumping, in any situation where the *average power* generated in the first or higher order Stokes becomes significant (typically for average powers >1 W), thermal loading of the Raman medium itself becomes significant, and the consequential thermal lensing must be accounted for in the design of Raman resonators.

Thermal loading in crystalline Raman materials has previously been dealt with in detail by Pask [18]. Every Stokes photon generated in the Raman medium results in $\hbar\omega_R$ vibrational energy deposited in the medium within the mode volume of the Stokes field. The heat deposited (average power) in the Stokes mode volume is thus

$$P_{\text{heat}} = P_{s1}\left(\frac{\lambda_{s1}}{\lambda_L} - 1\right)$$

where P_{s1} is the first-Stokes average power, and λ_{s1} and λ_P are the first-Stokes and pump wavelengths, respectively. Assuming TEM_{00} mode for the first-Stokes field (with $1/e^2$ Stokes mode radius in the Raman crystal ω_{S1}) the thermal lens power arising in the Raman crystal from the thermooptic effect (i.e., ignoring thermoelastic effects and end face curvature, which are generally small) can be calculated as

$$\frac{1}{f_{\text{thermal}}} = \left(\frac{dn}{dt}\right)\frac{1}{k_C}\frac{P_{S1}}{\pi\omega_{s1}^2}\left(\frac{\lambda_{S1}}{\lambda_p} - 1\right).$$

The thermal lens power is seen to scale with the average power of the first-Stokes line and the thermooptic coefficient (dn/dT) of the Raman crystal and inversely as the Stokes mode radius (squared) and thermal conductivity (k_C) of the crystal. Obviously, second or higher Stokes generation incurs higher energy defect, and therefore, correspondingly stronger thermal lensing.

Table II lists data related to the thermal properties of common Raman crystals. We see that for high average power SRS, the best of the common Raman crystals are KGW, YV (and GV), and BW, the vanadates having superior thermal conductivity but KGW having the lowest thermooptic coefficient. It is notable that the thermooptic coefficient dn/dT is generally *negative* for the tungstates BN and LI; thus, the thermal lenses formed have *negative* lens powers for these crystals (although we cannot find a value for dn/dT for BW in the literature, we expect it is negative and similar to that for calcium tungstate). For KGW, dn/dT

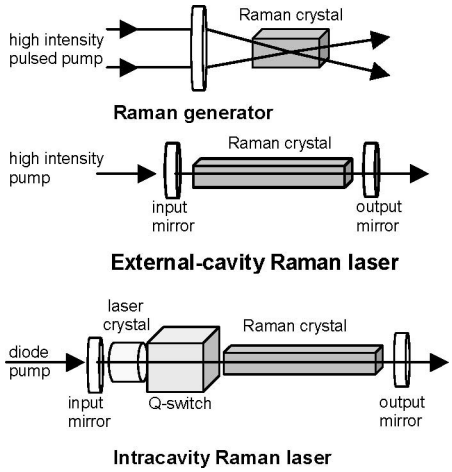

Fig. 1. Raman laser configurations.

can be *positive or negative* depending on the crystal orientation relative to pump polarization, and in fact, several athermal crystal orientations for KGW have been identified by Mochalov [33] and Biswal *et al*. [34]. The vanadates form positive thermal lenses as does YAG and many common laser crystal hosts.

In situ measurements of thermal lens power for Raman crystals (LI and BN) thermally loaded by SRS have been conducted by Reverman *et al*. [35] and Pask *et al*. [36] using lateral shearing interferometry to measure the wavefront of a probe beam passing through the Stokes mode volume. Focal lengths of -25 and -12.5 cm respectively were measured at average Stokes powers of 1 W (corresponding to average power densities $\sim 8 \times 10^6$ W/m^2) in good agreement with the theory. Although there are no comparable measurements for KGW, results of intracavity Raman laser experiments using KGW [16] indicate that thermal lensing due to SRS thermal loading is at least an order of magnitude weaker than that for LI.

The consequences of thermal lensing due to SRS thermal loading of the Raman crystal can be quite significant for resonator design of both external cavity and intracavity Raman lasers. We discuss these issues in more detail in the following sections relating to specific Raman laser configurations.

IV. Raman Laser Configurations

There are three different configurations for SRS frequency conversion of pump lasers, as illustrated in Fig. 1. *Raman generators* involve single-pass conversion of high-peak-power pulses of duration usually in the 10–100 ps (but sometimes also in the nanosecond) domains. In the steady-state regime, the Stokes signal grows from spontaneous Stokes noise as $\exp(g_R I_P z)$, thus, longer (40–50 mm) Raman crystals are preferred as long as the pump mode diameter does not vary significantly over the full crystal length. In order to reach the threshold for SRS, the incident pump beam is usually focused into the Raman crystal to reach pump intensities $\sim$1 GW/cm^2, at which level crystal damage and the onset of competing nonlinear processes (especially self-focusing) are likely for many candidate Raman crystals. At these very high pump intensities, it is also common to observe SRS to multiple-Stokes orders and several anti-Stokes orders. In some situations, it is useful to add a reflecting mirror at the pump and Stokes wavelengths immediately after the Raman crystal to get a double-pass for the pump and Stokes emission [19].

External cavity (alternatively called *external resonator*) *Raman lasers* involve placing a resonator (for the Stokes wavelengths) around the Raman crystal, which is pumped by an external laser source through the input mirror, where the latter highly reflects at the Stokes wavelengths. The Stokes-shifted Raman output is coupled via the output mirror, which generally has up to 50% transmission at the Stokes wavelengths for high-power (usually nanosecond) pulse pumping at low pulse-repetition frequencies (PRF $\sim$10 Hz), intermediate values ($\sim$10%) for pulse-pumping in the nanosecond domain at high PRF ($\sim$10 kHz), and low transmission ($<$1%) for CW external cavity Raman lasers.

Threshold for SRS is reached when the round-trip steady-state Raman gain exceeds the round-trip resonator losses, i.e.

$$R_1 R_2 \exp\left(2 g_R I_P L\right) \geq 1$$

where R_1 and R_2 are the reflectivities of the input and output mirrors, respectively, at the Stokes wavelength(s), and L is the length of the Raman crystal (assuming the resonator losses are dominated by mirror transmission). Resonating the Stokes signal reduces the effective pump intensity required to reach the threshold; Pask [18] has calculated that first-Stokes SRS threshold for a 50-mm-long BN crystal in a resonator with $R_1 R_2 > 0.6$ is reached at only $I_P \sim 5$ MW/cm^2. The output mirror is often coated for high reflectivity at the pump wavelength to double-pass the pump; mirror coatings may be specified to couple out the first-Stokes line, to resonate the first-Stokes and couple out the second-Stokes, to resonate both the first- and second-Stokes and to couple the third-Stokes, to obtain output on several Stokes orders simultaneously, or to achieve other desired spectral content of the output. Thermal lensing due to SRS heating of the Raman crystal at high average powers ($>$1 W) must be considered in the design of the Raman resonator to ensure resonator stability over the operating range of pump and Stokes output powers and to match the pump and Stokes modes in the crystal at the maximum Stokes power to achieve the maximum optical conversion efficiency. A simple consequence of the negative thermal lensing of many of the Raman crystals of choice is that plane—plane resonators become unstable just as soon as SRS threshold is reached.

Intracavity Raman lasers involve placing the Raman crystal within the optical cavity (resonator) of the pump laser itself. In this case, the laser crystal is pumped by an external source, for example, flashlamps, or for *all-solid-state lasers*, by high-power semiconductor diode lasers either arranged in side-pumping or end-pumping configurations (diode-end-pumping through the input mirror is shown in Fig. 1). To avoid confusion in describing intracavity solid-state Raman lasers it is normal to call the wavelength of the "pump" laser the "fundamental" (e.g., the fundamental for Nd:YAG is usually at 1064 nm). The resonator has high-Q (low-loss) at the fundamental and the generated Stokes line is coupled out through the output mirror. As for external cavity Raman lasers, the mirror coatings of intracavity Raman lasers may be specified such that the resonator also has high-Q at the first-Stokes while the second-Stokes line is coupled

from the output mirror (and so on). An intracavity Q-switch enables very high peak circulating powers of the fundamental to be generated, enabling SRS threshold to be reached in most of the commonly used Raman crystals at quite moderate overall input/output powers (for example, in an Nd:YAG laser end-pumped with a 20-W diode and acousto-optic (AO) Q-switched at 20 kHz with a high-Q cavity, it is quite easy to generate peak circulating powers up to $\sim$1 MW corresponding to intracavity intensities at the fundamental $\sim$1 GW/cm^2).

Resonator design in the case of intracavity Raman lasers is considerably more complex than that for external cavity Raman lasers. Thermal loading of the "fundamental" laser crystal is invariably present, and generation of significant average power at the Stokes wavelength(s) heats the Raman crystal (the thermal lens in the Raman crystal depends on the Stokes output power and is most often negative, whereas the thermal lens in the laser crystal depends on the (diode-pump) input power and is most often positive). The resonator must remain stable over the full range of operating input and output powers, and mode sizes in both the laser and Raman crystals need to be optimized to achieve good overall conversion efficiencies from the external (diode) pump source to Raman output. Note also that specification of mirror coatings for intracavity Raman lasers is more complicated than that for external cavity lasers; for example, the input mirror of a diode-end-pumped device must have high transmissivity at the pump wavelength but high reflectivity at both the fundamental *and* Stokes wavelength(s). Further, mirror coatings (and antireflection (AR)-coatings to crystals) should be specified to have high damage threshold, typically $>$100 MW/cm^2 for nanosecond pulses.

There are some important variations of the configuration of intracavity Raman lasers. In *coupled-cavity Raman lasers*, the Raman crystal is placed within the resonator for the fundamental wavelength (and therefore, benefits from the high circulating powers at the fundamental), but usually by means of a dichroic mirror, has a distinct Raman resonator (not shared by the laser crystal). *Intracavity self-Raman lasers* have a laser crystal, which also provides strong Raman gain (e.g., Nd:YV or GV). Obviously, these have the advantage of eliminating the need for a separate Raman crystal, but while this simplifies resonator design, thermal loading of the combined laser/Raman crystal is exacerbated at high average (SRS) powers, and design options to offset the effects are limited.

Perhaps the ultimate level of complexity of crystalline Raman lasers is reached with *intracavity frequency-doubled Raman lasers*. Here, a nonlinear crystal LiB_3O_5 (commonly LBO) cut for second-harmonic or SFG is added to the intracavity Raman laser resonator.The mirror coatings provide high-Q at both the fundamental and the first-Stokes wavelengths (possibly also the second-Stokes wavelength) but transmit the SHG or SFG output in the visible. The resonator must be designed to accommodate thermal lensing in both the laser and Raman crystals, and additionally needs to ensure that the mode size in the SHG/SFG crystal is appropriate over the range of operating conditions.

CW intracavity Raman lasers are a very recent development; the Q-switch is eliminated but detailed consideration of the resonator design, to achieve small mode sizes under circumstances of high thermal loadings and mirror coating specifications such that there are very low losses at the fundamental, is essential. Despite the added design complexities of intracavity frequency doubling, the authors and coworkers have recently demonstrated for the first time efficient all-solid-state CW yellow sources based on intracavity frequency-doubled CW crystalline Raman lasers [37].

Typical performance characteristics of crystalline Raman lasers in their different configurations are summarized in the following sections with an emphasis on latest results.

V. Raman Generators

Tabulations of past results for SRS of high-power picosecond and nanosecond pulses in single- and double-pass Raman generators have been given by both Basiev and Powell [17] and Pask [18]. The most comprehensive study of the past five years has been that undertaken by Cerny *et al*. [19], involving detailed measurements of Raman thresholds, gains, and conversion efficiencies for the key crystals KGW, KYW and BW, for both high-power picosecond (35–55 ps) and nanosecond (25 ns) pulse pumping at 1064, 532, and 355 nm, in single- and double-pass configurations. While BW has greatly superior gain compared to that of KGW and KYW in the steady-state regime, the gain for short-pulse pumping ($\tau_P \sim 40$ ps) is considerably reduced due to its rather longer dephasing time $T_R \sim 6.6$ ps compared to that of KGW and KYW ($T_R \sim 2$ and 1.6 ps, respectively). However, these are all much superior to BN in the short-pulse domain (for BN $T_R \sim 28$ ps). Although the steady-state gain for KGW is less than that of BW, in practice, conversion efficiencies for KGW are if anything superior to those of BW, reaching 50% for nanosecond pulses in the near infrared. We note that the highest SRS efficiency achieved for a Raman generator to date has been a peak-power conversion of 85% (effectively at the quantum limit) of 35-ps, 532-nm pump pulses to the first-Stokes at 560 nm in BW arranged in a double-pass configuration [38].

Application of SRS in crystal materials to frequency-shift Nd^{3+} lasers into the 1.5-μm eye-safe spectral region has been pursued for a number of years, but recently, Basiev *et al*. [39] have also reported efficient (10% optical) single- and double-pass Raman-shifting of high-power nanosecond pulses in the near infrared into the 1.5–2.2 μm spectral region. Subsequently, a high-power (100-mJ, 10-ns) source at 1.56 μm (obtained from a Q-switched Nd:YAG laser using a D_2 Raman shifter) has been used to demonstrate SRS in BW out to the fourth-Stokes at 3.69 μm, well into the midinfrared [40].

VI. External Cavity Raman Lasers

Use of optical cavities to enhance SRS conversion efficiencies by resonating the Stokes fields in crystals driven by external pump sources offers important benefits in the case of nanosecond pulses; resonating the Stokes signal lowers the pump intensities necessary to reach the SRS threshold, and increases extraction efficiency. External cavity configurations are very attractive for efficient SRS conversion of stand-alone pulsed (usually Q-switched) Nd^{3+} lasers for specific applications, especially to access the eye-safe near infrared around 1.5 μm and

the yellow orange regions of the visible spectrum, and by SHG, the ultraviolet, for a range of remote sensing applications.

A. External Cavity Crystalline Raman Lasers Based on Barium Nitrate

Nanosecond Raman lasers operate in the steady-state SRS regime, for which choice of Raman crystal is motivated primarily by considerations of high Raman gain, and thus, BN has been used extensively in external cavity configurations in the past [17], [18], [41], [42]. Near infrared and visible output pulse energies of several millijoules up to 100 mJ with pump Stokes efficiencies in the range of 25%–60% have been achieved at pulse rates up to a range of a few tens of hertz. In some situations (e.g., for small pump beam sizes ($\sim$1-mm diameter) and average Stokes powers $\sim$100 mW), adverse effects due to thermal loading of the Raman crystal have been observed but these could often be overcome simply by using higher beam diameters.

More significant thermal loading problems for a BN external cavity Raman laser pumped by a Q-switched Nd:YAG laser have been identified by Takei *et al.* [43]. For the first-, second-, and third-Stokes output energies of 28, 27, and 8.5 mJ, respectively, at PRF 20 Hz (corresponding to somewhat over 1.2-W average Stokes power), significant thermal lensing in the BN crystal was observed, the Raman outputs dropping rapidly as the crystal was heated in the first 100 s of laser operation. The (negative) thermal lens arising in the BN crystal was subsequently determined, and resonator mirror curvatures were altered to improve matching of the pump and Stokes modes within the crystal, ultimately to achieve 15.5% conversion to the third-Stokes in continuous operation of the laser.

The authors of this paper and coworkers [44] have reported studies of external cavity BN Raman lasers pumped by a compact (diode-pumped) AO Q-switched Nd:YAG laser operating at 4 kHz and delivering 3 W at 1064 nm. For the rather low peak powers ($\sim$100 kW) of this pump, the pump mode diameter in the Raman crystal is necessarily small (160 μm) to enable Raman threshold intensities to be reached. For a resonator geometry chosen to match the Stokes mode to the pump mode at low incident powers (near threshold), the strong thermal lens, which forms in the BN crystal at the upper limit of pump power (1.3-W Stokes output) results in almost doubling of the Stokes mode diameter, with consequential degradation in output beam quality due to aberrations in the crystal. While redesign of the resonator to mode-match in the presence of strong thermal lensing at high Stokes powers is expected to give significant improvement in output beam quality, we believe that the high-gain coefficient of BN is outweighed by its generally poor thermal properties (including thermally induced birefringence) in this application.

We note finally that Ermolenko *et al.* [45] have recently reported a novel externally pumped BN Raman laser using an *unstable* resonator to circumvent thermal degradation and achieve high output beam quality at first-Stokes (563 nm) pulse energies 34 mJ at 10 Hz PRF. The first-Stokes beam quality was sufficient for external SHG in KD_2PO_4 to generate UV 281-nm pulses of 4. 2 mJ at $\sim$12% efficiency.

B. External Cavity Crystalline Raman Lasers Based on Tungstates

Although the tungstates have lower steady-state Raman gain than BN, the superior thermal properties make them very attractive for application to SRS frequency conversion of high average power or high pulse energy sources. The superior overall characteristics of BW have been exploited in recent studies of high-energy and high-power external cavity Raman lasers reported by Basiev *et al.* [46]. For a conventional Raman resonator with 45% coupling at the first-Stokes wavelength (1180 nm) pumped by a large-scale Nd:YAG laser delivering an eight-pulse-train comprising 145-mJ, 50-ns pulses separated at 50-μs intervals at 30-Hz repetition rate of the pulse-train (average power $\sim$35 W), total Stokes power output was 7.65 W comprising 5 W on the first-Stokes, 2.4 W on the second-Stokes (1325 nm), and 0.25 W on the third-Stokes (1.510 nm) at overall pump-Stokes efficiency 28%. Using a large-scale Nd:GGG laser providing a 50-pulse-train comprising individual 380-mJ pulses of duration 50 ns and separated by 50 μs (19 J in total) resulted in total Stokes output of 1.6 J at the first-Stokes and 0.43 J at the second-Stokes lines.

Somewhat at the other end of the scale, Mildren *et al.* [47], [48] have reported investigations of Raman frequency conversion of low average power (1–3 W), high-PRF, diode-pumped frequency-doubled Nd:YAG lasers using external cavity Raman configurations based on KGW. The pump beam was focused through the input mirror to a 160-μm-diameter beam waist in the 50-mm-long b-cut KGW crystal. The Raman resonator mirrors had concave radii of curvature $\sim$200 mm and were spaced by 60 mm to give best matching of the Stokes modes to the pump mode at full operating power. The input mirror had high transmissivity for the 532-nm pump but high reflectivity for the various Stokes lines up to the fourth-Stokes; a variety of coupling mirrors were used to generate outputs with different spectral content. For example, simultaneous output at five wavelengths was obtained using a broadband coupler having $\sim$50% transmissivity from 520–660 nm; total average power output on the four Stokes lines (559, 589, 622, and 658 nm) of the 901-cm^{-1} Raman mode was 1.68 W, the balance of the 2.36-W, 532-nm pump also emerging colinear with the Raman output. Average powers on the individual Stokes lines ranged from 400 mW at 559 nm to 130 mW at 658 nm, and total SRS conversion efficiency was 71%. Accessing the two Raman modes, 768 and 901 cm^{-1}, was achieved simply by rotating the KGW crystal by 90° about the b-axis such that the pump polarization was parallel with either the Ng or Nm crystal axes. Alternatively, output couplers could be chosen to efficiently generate a single Stokes output wavelength. For example, using an output coupler with high reflectivity at the first-Stokes, but high transmissivity (50%–70%) in the yellow region, frequency conversion into either of the two second-Stokes lines (579 and 589 nm) could be selected with conversion efficiencies 58% (68% slope) and 64% (78% slope) for the 2.4-W pump. A very recent extension of this work by Mildren [49] has involved addition of an intracavity b-Barium-Borate (BBO) crystal cut for SHG/SFG at 280 nm to an external cavity KGW Raman laser pumped by standard 532-nm

sources to achieve wavelength-selectable output amongst more than eight UV wavelengths ranging from 266 to 320 nm with average powers in the range of several tens of milliwatts and pulse energies up to 0.22 mJ for individual lines.

Extensive studies including modeling of external cavity Raman lasers based on KGW and pumped by a Q-switched Nd:YAG laser in the near infrared have been reported recently by Ding *et al*. [50].

VII. Intracavity Crystalline Raman Lasers

A. Near Infrared Stokes-Raman Lasers

Though the advantages of using intracavity configurations for crystalline Raman lasers, especially for frequency conversion of low peak power, high-PRF sources were recognized by Ammann [2]–[4] in the earliest years of Raman laser development, it was not until almost 20 years later that this configuration began to be fully exploited. (Though the first studies of self-Raman laser materials Nd:KYW and Nd:KGW reported by Andryanus *et al*. in 1985–1986 [10] inevitably also involved intracavity configurations.). New interest in intracavity Raman lasers was triggered by the report of Murray *et al*. in 1995 [14] of an intracavity BN Raman laser based on a flashlamp-pumped Nd:YAG laser gain module and emitting in the 1.5-mm eye-safe band. This was followed by the first report [51] of an all-solid-state intracavity Raman laser, which is based on a 5-W fiber-coupled diode-end-pumped Q-switched Nd:YAG /$CaWO_4$ intracavity Raman laser (as shown in Fig. 1). The latter device was both compact and efficient, giving 480-mW average output power on the first-Stokes line (1178 nm) at 10-kHz PRF.

The intracavity configuration for crystalline Raman lasers is very well matched to the normal operating regime of CW diode-pumped, Q-switched solid-state lasers; these generally give relatively low peak power (10 s–100 kW) output pulses but the circulating power within a high-Q resonator is much higher, and this can be used effectively in intracavity SRS to obtain high overall conversion efficiencies to Stokes output. Following our own work on intracavity LI Raman lasers based on arc-lamp-pumped Nd:YAG gain modules and high-PRF Q-switching giving 1.7 W at the first-Stokes (1155 nm) also reported in 1998 [52], we went on to demonstrate an all-solid-state intracavity LI Raman laser based on a diode-double-end-pumped Nd:YAG rod with AO Q-switch, giving a record 2.7-W average power on the first-Stokes line (1155 nm) at an estimated 10% overall optical conversion efficiency (diode Stokes efficiency) [15]. A detailed study of temporal, spatial, and spectral characteristics of diode-pumped intracavity LI Raman lasers was reported subsequently [28].

Also, at this time, Grabtchikov *et al*. [53] reported the first diode-pumped self-Raman laser, a miniature Nd:KGW laser pumped by a 1-W CW diode and passively Q-switched by a Cr^{4+}:YAG saturable absorber. The laser gave 4.8-mW average power in 23-ns pulses at 1 kHz on the 1181-nm first-Stokes of KGW from the 1057-nm fundamental at 0.7% diode Stokes efficiency. This was followed quickly by a report from Lagatsky *et al*. [54] of a miniature Yb:KGW self-Raman laser of similar design, giving 7 mW on the first-Stokes (1139 nm) but at improved efficiency of 2% from the diode pump. Coincidentally, Findeisen *et al*. [55] had demonstrated self-Raman operation (on the alternative first-Stokes at 1162 nm) of a quasi-CW diode-side-pumped Nd:KGW laser.

From this starting point, there has been a rapid expansion of research in all-solid-state (i.e., diode-pumped) intracavity crystalline Raman lasers. Table III lists performance data from a number of key reports from 1998 to the present; there are many combinations of laser and Raman crystals represented. These include intracavity Raman lasers with discrete laser and Raman crystals, and self-Raman lasers integrating the two, and all are Q-switched devices involving either active (usually AO) or passive Q-switching (usually based on Cr^{4+}:YAG).

Self-Raman lasers are ideal for miniaturization, and for the most part, these are passively Q-switched at high PRF, usually giving subnanosecond pulse durations. Such devices generally require only modest diode-pump power of 1–2 W, but despite this, diode Stokes conversion efficiencies have reached up to 7% [64] and average powers up to 400 mW [66]. Note that, however, passively Q-switched intracavity Raman lasers using separate laser and Raman crystals have also demonstrated very good performance, for example, the Nd:LSB/BN laser reported by Demidovich *et al*. [59], which has diode Stokes conversion efficiency of 8% for 118-ps pulses at 83 kHz.

For the most part, devices giving high average power ($>$1W) Stokes output use discrete laser and Raman crystals since these generally operate under conditions where strong thermal loading of the Raman medium is experienced, and using the discrete components allows more options in thermal management. The highest average power achieved to date for diode-pumped intracavity Raman lasers, i.e., 2.6 and 3.0 W have also been reported for first-Stokes outputs of Nd:YAG/LI and BN lasers [15], [18], respectively. Although KGW has considerably lower steady-state gain than BN, its superior thermal characteristics make it much more tolerant to thermal loading, resulting in order-of-magnitude weaker thermal lensing than either LI or BN. We have obtained first Stokes output powers (1176 or 1158 nm) of around 1.9 W at 10% conversion efficiency, limited by the availability of mirrors optimized for near infrared Stokes output; we predict higher powers (e.g., around 4–5 W) should be achievable with appropriate mirrors. High average powers (1.6 W) at diode Stokes conversion efficiency of 16.9% have also been reported recently for an Nd:YAG/BW laser with active Q-switching. Problems with thermal loading were not observed (BW and KGW have similar thermal properties) but optical damage due to self-focussing was encountered and may limit further power scaling [65]. Notable powers have also been reported [62], [63] for self-Raman lasers based on diode-pumped Nd:YVO_4 with active Q-switching. Also, 1.5 and 1.2 W respectively were obtained for the first-Stokes lines at 1176 and 1525 nm from the 1064- and 1342-nm fundamentals obtained with appropriate mirror selection. High thermal loading of the laser/Raman crystal resulted in strong thermal lensing and other effects attributed to temperature-dependent broadening of the Raman linewidth.

The effects of thermal lensing in both the laser and Raman crystal on the efficiency of intracavity Raman lasers have been

TABLE III
PERFORMANCE OF SELECTED INTRACAVITY CRYSTALLINE RAMAN LASERS, INCLUDING SELF-RAMAN LASERS

Diode power	Laser crystal	Raman crystal	λ 1st-Stokes	pulse width	*prf*	Stokes power	Efficiency	Year/Ref
5W	Nd:YAG	$CaWO_4$	1178nm	6ns	10kHz	0.5W	9%	1998 [52]
30W	Nd:YAG	$LiIO_3$	1156nm	20ns	10kHz	2.6W	9%	1999 [15,28]
0.7W	Nd:KGW	$\{KGd(WO_4)_2\}$	1181nm	23ns	1kHz	4.8mW	0.7%	1999 [54]
0.37W	Yb:KGW	$\{KGd(WO_4)_2\}$	1139nm	20ns	20kHz	7mW	2%	2000 [55]
90mJ	Nd:KGW	$\{KGd(WO_4)_2\}$	1162nm	50ns	47Hz	0.1mJ	0.1%	2000 [56]
4mJ	Nd:$PbWO_4$	$\{PbWO_4\}$	1171nm	8ns	50Hz	2.5mJ	<0.1%	2001 [57]
30W	Nd:YAG	$Ba(NO_3)_2$	1197nm	15ns	10kHz	3W	10%	2001 [18]
1.6W	Nd:YVO_4	$Ba(NO_3)_2$	1197nm	15ns	32kHz	111mW	6.9%	2002 [58]
60mJ	Nd:YAG	$BaWO_4$	1169nm	3.5ns	14Hz	2.3mJ	4.4%	2002 [59]
1.1W	Nd:LSB	$Ba(NO_3)_2$	1196nm	118ps	83kHz	90mW	8%	2003 [60]
10W	Nd:YVO_4	$KGd(WO_4)_2$	1497nm	25ns	15kHz	200mW	2%	2004 [61]
			1528nm	25ns	15kHz	100mw	1%	
0.52W	Nd:YVO_4	$\{YVO_4\}$	1180	<0.8ns	55kHz	20mW	4%	2004 [62]
10.8W			1176nm	18ns	20kHz	1.5W	13.9%	2004 [63]
13.5W			1525nm	6ns	20KHz	1.2W	8.9%	2004 [64]
2W	Nd:$GdVO_4$	$\{GdVO_4\}$	1176nm	750ps	22kHz	140mW	7%	2004 [65]
19W	Nd:YAG	$KGd(WO_4)_2$	1158nm	30ns	15kHz	1.9W	10%	2005
10W	Nd:YAG	$BaWO_4$	1181nm	24ns	20kHz	1.6W	17%	2005 [66]
7W	Yb:$KLu(WO_4)_2$	$\{KLu(WO_4)_2\}$	1138nm	0.7ns	28kHz	0.4W	5.7%	2005 [67]
1.5W	Nd:$PbMoO_4$	$\{PbMoO_4\}$	1163nm	<0.5ns	7.5kHz	45mW	3%	2006 [68]
30mJ	Nd:$BaWO_4$	$\{BaWO_4\}$	1169nm	1.3ns	5Hz	0.8mJ	2.7%	2006 [69]
1.2J	Nd:YAG	$KGd(WO_4)_2$	1522nm	2ns	30Hz	50mJ	4%	2006 [70]

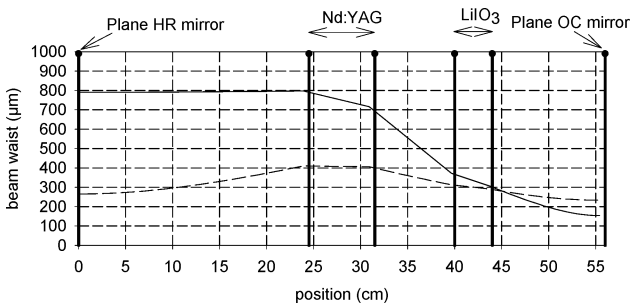

Fig. 2. Ray-trace for intracavity Nd:YAG/LI Raman laser for laser operation on the fundamental only (trace 1) and for operation on the fundamental and first-Stokes (trace 2).

discussed in detail by Pask [18]. To achieve high average power and high efficiency, it is necessary to design the laser resonator such that cavity mode sizes give good matching to the diode-pump mode in the laser crystal and maintain the necessary high intensities in the Raman crystal (both in the same place in the case of self-Raman lasers). Fig. 2 gives an example of a resonator, which is stable and has good mode-matching in the absence of thermal loading of the Raman crystal (in this case of LI) but for which the mode size at the laser crystal (Nd:YAG) rapidly expands (resulting in poor pump mode-matching and ultimately leading to resonator instability) as a strong negative thermal lens in the Raman crystal forms due to SRS heating.

The complex spatial and temporal interactions between the fundamental and Stokes fields within intracavity Raman lasers commonly result in gain-switching, self-mode-locking, and chaotic self-pulsation on the one hand, and Raman beam clean-up (manifests in a single-transverse-mode Raman output for multi-transverse-mode pump) on the other. These have been analyzed by Band *et al*. [70] in the case of temporal instabilities (see also Murray *et al*. [71]), and Murray *et al*. [72] in the case of Raman beam clean-up in crystalline Raman lasers, and examples of both effects are shown by Pask [18]. In the experience of the authors, stable, reproducible, and reliable operation of Q-switched intracavity Raman lasers operating at multiwatt average powers is not difficult to achieve.

VIII. INTRACAVITY FREQUENCY-DOUBLED RAMAN LASERS FOR VISIBLE OUTPUT

While the pulsed output from Raman lasers in their different configurations can be externally frequency-doubled, for the aforementioned diode-pumped intracavity Raman lasers, this generally results in quite low overall optical conversion efficiency. Intracavity SHG (or SFG) of the Stokes lines in intracavity Raman lasers takes advantage of the high circulating

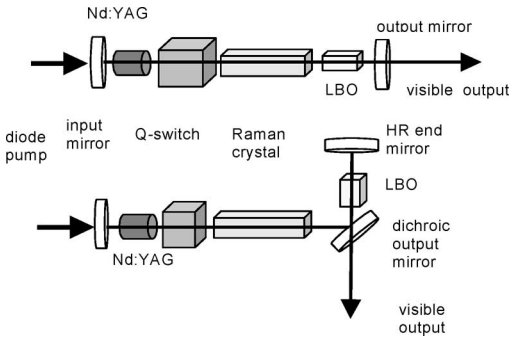

Fig. 3. Intracavity frequency-doubled crystalline Raman lasers.

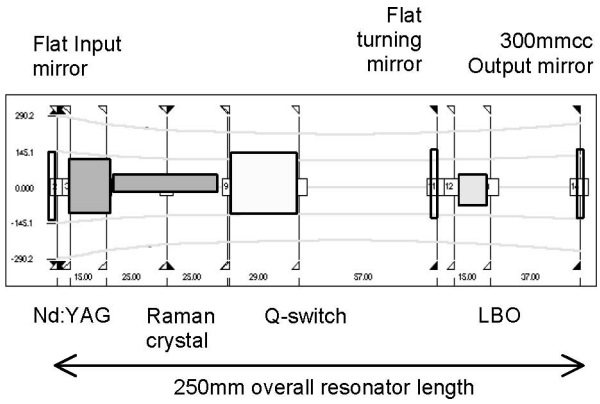

Fig. 4. Ray-trace for optimized resonator design for intracavity frequency-doubled diode-pumped Nd:YAG/LI Raman laser in the presence of strong thermal lensing in the laser and Raman crystals.

Stokes power for efficient nonlinear conversion to the visible. Effectively, the SHG/SFG acts as nonlinear coupling of the Stokes field via the visible output. Intracavity SFG allows additional wavelengths to be generated by mixing of the fundamental and the first-Stokes, the first- and second-Stokes, or other combinations.

Fig. 3 shows schematics of the common resonator configurations for intracavity SHG/SFG crystalline Raman lasers. The simplest configuration [Fig. 3(a)] is merely to add the nonlinear crystal into a linear intracavity Raman resonator, the output mirror having high reflectivity at the fundamental and first-Stokes, possibly also at the second- or higher order Stokes wavelengths, and high transmissivity at the visible SHG/SFG wavelengths. This configuration was used by Ammann [4] in the first demonstration of an intracavity frequency-doubled Raman laser, although in that case, the LI Raman crystal was also cut for SHG/SFG from near infrared to visible, thus, filling the role of both Raman shifter and frequency doubler. The disadvantage of the simple two-mirror linear cavity is that the output mirror couples only the forward-propagating SHG/SFG visible beam, so that about half of the visible power is lost. In our own work on intracavity frequency-doubled Raman lasers, we have used a three-mirror folded (L-shaped) resonator [Fig. 3(b)], which provides a high-Q for the fundamental and Stokes wavelengths, while the visible SHG/SFG output is efficiently coupled out via the dichroic turning mirror. We have undertaken systematic design studies of the folded laser resonator to optimize conversion efficiency by ensuring that the mode sizes at each of the three key components are of the correct size for efficient extraction of the fundamental from the diode pump mode in the laser crystal, efficient SRS in the Raman crystal, and efficient SHG in the nonlinear crystal, taking account of thermal lensing in the laser and Raman crystals at the maximum input/output powers. Fig. 4 shows a ray-trace for the optimized resonator. It is generally true that the mode size is the highest for the laser crystal and the lowest for the nonlinear SHG/SFG crystal for the best laser performance.

This resonator design optimization resulted in significant improvements to overall diode-yellow power conversion efficiencies, which reached 7% for 1.4-W 578-nm output from the purpose-engineered diode-pumped intracavity Nd:YAG/LI/LBO frequency-doubled Raman laser [73]. More recently, replacement of the LI Raman crystal with KGW and resonator redesign, to take account of the substantially better thermal characteristics of the latter, have resulted in yellow (579 nm) output powers up to 1.8 W at diode-yellow conversion efficiency 9% [16].

For intracavity frequency-doubled Raman lasers the cascaded nature of SRS process can be utilized to generate wavelength-selectable output at multiple wavelengths in the green yellow red spectral regions [74]. In an intracavity Raman laser, the fundamental optical field at 1064 nm is cavity-dumped through the nonlinear process of SRS (as the resonator mirrors are chosen to provide high-Q at the fundamental). Given sufficiently broad mirror coatings, the fundamental, first, second, and potentially higher order Stokes wavelengths can all be resonated. This "cascading" of the SRS process in combination with a nonlinear crystal, which can be configured by angle or temperature tuning to frequency-double the fundamental, the first Stokes, the second Stokes, or sum the frequency of a pair of these, output across a range of discrete visible wavelengths can be obtained. LBO (angle- or temperature-tuned) and BBO (angle-tuned) are both suitable choices for the nonlinear medium. In recent work by Mildren *et al*. [16], we reported that by (type I) angle tuning the intracavity LBO frequency doubler, we can switch easily from 1.8 W at 579 nm to 0.95 W at the sum-frequency (555 nm) to 1.7 W at 532 nm, the second-harmonic of the fundamental. For the alternative Raman mode (901 cm^{-1}) of KGW, switching from 588 to 559 nm, and then from 559 to 532 nm is equally possible, as is SFG of the first- and second-Stokes (to 606 or 621 nm, depending on the Raman mode), SHG of the second-Stokes, and so on, depending on mirror coating tranmission.

IX. CW Raman Lasers

The most recent, and perhaps the most significant, development of crystalline Raman lasers in the past three years has been that of CW Raman lasers. Although CW fiber and semiconductor Raman lasers are well-known, the first CW bulk insulating crystalline Raman laser was reported only in 2004 by Grabtchikov *et al*. [75]. Here, a CW argon ion laser giving 10 W at 514-nm-pumped BN Raman crystal was placed in a concentric external resonator (high-finesse $\sim$1000 for the first-Stokes at 543 nm), the pump undergoing a double-pass before exiting the input mirror. Careful attention was paid to matching of the pump

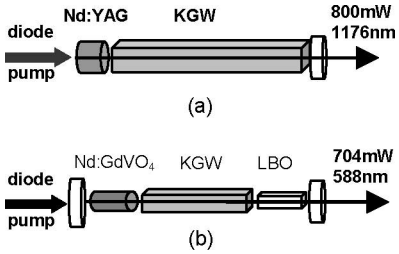

Fig. 5. Schematics of (a) CW intracavity Nd:YAG/KGW laser and (b) CW intracavity Nd:$GdVO_4$/KGW laser with intracavity frequency doubling in LBO.

mode ($\sim$120 μm diameter) to the Stokes mode in the Raman crystal at the maximum Raman output power, taking account of thermal lensing in the BN due to SRS heating. Threshold for CW first-Stokes laser operation was 2 W, and the maximum power at 543 nm was 164 mW at 5.5-W pump.

The first all-solid-state (diode-pumped) crystalline Raman laser was reported in 2005 by the same group. Demidovich *et al*. [76], taking advantage of the low cavity losses afforded by using a self-Raman laser material in an intracavity configuration, used a 2.4-W fiber-coupled diode imaged to a 150-μm-diameter pump mode in Nd:KGW. The input mirror, which was coated directly on the first Nd:KGW crystal face, and the output mirror had round-trip transmission losses at the fundamental (1067 nm) and first-Stokes (1181 nm) of only $\sim$0.14% and 0.43%, respectively. The cavity was close to hemispherical with the output mirror concave radius of curvature (ROC = 50 mm). Fundamental and first-Stokes threshold were reached for diode pump power of 55 mW and 1.15 W, respectively, and the maximum 1181-nm output of 54 mW (total from both input and out mirrors) was reached at pump power of 2.06 W, corresponding to diode Stokes efficiency 2.6%. Orlovitch *et al*. [77] have subsequently reported 178-mW CW output on the first-Stokes line (1177 nm) for a diode-pumped Nd:YVO_4/$PbWO_4$ Raman laser with 2.3-W pump, representing substantially higher efficiency of $\sim$7.7%.

Concurrently, Pask [78] has demonstrated power scaling of a diode-pumped CW intracavity Raman laser toward the 1 W level; the laser resonator is shown schematically in Fig. 5(a). The output of a high-power fiber-coupled diode laser was imaged approximately 1:1 from the 400-μm-diameter fiber into the Nd:YAG fundamental laser crystal through the input mirror, which was coated directly on the flat end face of the crystal. The Raman crystal was a 50-mm-long KGW crystal with AR-coatings for 1064–1150 nm. The output mirror was also flat and highly reflecting for the fundamental but 0.25% transmitting for the first-Stokes wavelength at 1176 nm. For pump power of 20 W, the thermal lens was estimated to be +100 mm, and the fundamental mode size in the Raman crystal (ignoring the relatively weak thermal lensing in the KGW) was then calculated to be 472 μm. For round-trip cavity loss of 1%, the intracavity fundamental power required to reach SRS threshold was then calculated to be $\sim$350 W, which is about half the value expected for the fundamental at 20-W diode pump. In the experiments, first-Stokes threshold was reached at 5 W, and the maximum 1176-nm output power of 800 mW was obtained at 20-W pump corresponding to diode Stokes efficiency of $\sim$4%.

A further key observation of these latter experiments was that the circulating power at the Stokes wavelength was $\sim$320 W, which is sufficiently high to encourage investigation of the potential for intracavity frequency doubling of the Stokes wavelength for CW visible generation. In fact, this has now been achieved for a diode-pumped Nd:$GdVO_4$ laser with intracavity KGW Raman and LBO frequency doubling crystals (see Fig. 5). The flat input and output mirrors had very low loss (tranmissivities $<$0.006% and $<$0.004%) at the fundamental and first-Stokes, but were 95% transmitting for the 588-nm second-harmonic of the first-Stokes. A maximum CW power at 588 nm (measured from the output mirror only) of 704 mW has been obtained for diode pump power of 13.7 W, representing a diode-yellow efficiency of 5.1% [37]. Strong thermal lensing in the laser crystal prevented fully CW operation above 14-W pump power but the potential to reach yet higher powers was demonstrated by applying 50% duty cycle to the pump; under these conditions, we observed 1.57-W quasi-CW power output in the yellow region for 20-W quasi-CW pump power. We believe that with improved resonator design and thermal management, CW powers in the yellow orange region of 2 W or more are feasible at diode-visible efficiencies approaching 10%.

For lower powers, the attractions of self-Raman materials are clear, and Omatsu *et al*. [79] have very recently demonstrated 92-mW CW yellow region at 588 nm, the second-harmonic of the 1176-nm first-Stokes, from a miniature (20-mm-long) diode-pumped Nd:YVO_4 self-Raman laser with intracavity SHG in LBO, with only 4.2-W diode pump power. High beam quality in the visible ouput (TEM_{00} with $M^2 \sim 1.1$) has been obtained with good long-term power stability, though fast amplitude fluctuations are apparent. We anticipate that CW intracavity frequency-doubled self-Raman lasers can be both scaled down to milliwatt visible powers for $\sim$1-W pump and up toward 1-W for $\sim$10-W pump.

X. Conclusion

Developments of crystalline Raman lasers have expanded rapidly in the past five years as SRS in crystals has been adopted as a highly efficient and practical means of extending the wavelength versatility of established laser systems. Recent focus has been on all-solid-state Raman lasers, which lever the capabilities of the latest generation of diode-pumped devices. There remain many opportunities for novel developments in high average power devices, exploiting parallels between Raman lasers and diode-pumped lasers, and for efficient wavelength extension into broader regions of the visible (blue-green) and the ultraviolet using intracavity SHG/SFG. We believe that CW Raman lasers also offer very exciting opportunities for research and development, especially of a new generation of wavelength-versatile CW visible sources. The authors believe that there is also the potential for novel Raman laser resonator configurations, which exploit the unique properties of Raman lasers; two examples that emerged recently include the use of unstable Raman resonators [45] and noncollinear fundamental and Stokes resonators [69].

ACKNOWLEDGMENT

J. Piper would like to thank the Carnegie Trust of the Universities of Scotland for the award of the Carnegie Centenary Professorship, and Heriot-Watt University, Edinburgh, the host institution during 2006 when this paper was written.

REFERENCES

[1] G. Eckhardt, D. P. Bortfeld, and M. Geller, "Stimulated emission of Stokes and anti-Stokes Raman lines from diamond, calcite and alpha-sulfur single crystals," *Appl. Phys. Lett.*, vol. 3, pp. 137–138, 1963.

[2] E. O. Ammann and J. Falk, "Stimulated Raman scattering at kHz pulse repetition rates," *Appl. Phys. Lett.*, vol. 27, no. 12, pp. 662–664, 1975.

[3] E. O. Ammann and C. D. Decker, "0.9-W Raman oscillator," *J. Appl. Phys.*, vol. 48, pp. 1973–1975, 1977.

[4] E. O. Ammann, "Simultaneous simulated Raman scattering and optical frequency mixing in lithium iodate," *Appl. Phys. Lett.*, vol. 34, pp. 838–840, 1979.

[5] A. S. Eremenko, S. N. Karpukhin, and A. I. Stepanov, "Stimulated Raman scattering of the second harmonic of a neodymium laser in nitrate crystals," *Kvantovaya Elektron.*, vol. 7, pp. 196–197, 1980.

[6] N. Bloembergen, "The stimulated Raman effect," *Amer. J. Phys.*, vol. 35, no. 11, pp. 989–1023, 1967.

[7] W. Kaiser and M. Maier, "Stimulated Rayleigh, Brillouin and Raman spectroscopy," *in Laser Handbook*, F. T. Arecchi and E. O. Schultz Dubois, Eds., Amsterdam, The Netherlands, p. 1077, 1972.

[8] C. S. Wang, "The stimulated Raman process," *in Quantum Electronics*, H. Rabin and C. L. Tang, Eds., New York: Academic, 1975, pp. 447–472, to be published.

[9] A. A. Penzkofer, L. Laubereau, and W. Kaiser, "High intensity Raman interactions," *Progress Quantum Electron.*, vol. 6, pp. 55–140, 1979.

[10] K. Andryunas, Y. Vishakas, V. Kabelka, I. V. Mochalov, A. A. Pavlyuk, G. T. Petrovskii, and Y. Syrus, "Stimulated-Raman self-conversion of $Nd3^+$ laser light in double tungstenate crystals," *JETP Lett.*, vol. 42, pp. 410–412, 1986.

[11] S. N. Karpukin and A. I. Stepanov, "Stimulated Raman scattering from the cavity under SRS in $Ba(NO_3)_2$, $Na(NO_3)$ and $Ca(O_3)$ crystals," *Sov. J. Quantum Electron.*, vol. 16, pp. 1027–1031, 1986.

[12] T. T. Basiev, V. N. Voitsekhovskii, P. G. Zverev, F. V. Karpushko, A. V. Lyubimov, S. B. Mirov, V. P. Morosov, I. V. Mochalov, A. A. Pavluik, G. V. Sinitsin, and V. E. Yakobson, "Conversion of tunable radiation from a laser utilizing an LiF crystal containing F2- color centres by stimulated Raman scattering in $Ba(NO_3)_2$ and $KGd(WO_4)_2$ crystals," *Sov. J. Quantum Electron.*, vol. 17, pp. 1560–1561, 1987.

[13] P. G. Zverev, J. T. Murray, R. C. Powell, R. J. Reeves, and T. T. Basiev, "Stimulated Raman scattering of picosecond pulses in barium nitrate crystals," *Opt. Commun.*, vol. 97, pp. 59–64, 1993.

[14] J. T. Murray, R. C. Powell, N. Peyghambarian, D. Smith, W. Austin, and R. A. Stolzenberger, "Generation of 1.5 μm: Radiation through intracavity solid-state Raman shifting in $Ba(NO_3)_2$ crystals," *Opt. Lett.*, vol. 20, pp. 1017–1019, 1995.

[15] H. M. Pask and J. A. Piper, "Efficient all-solid-state yellow laser source producing 1.2-W average power," *Opt. Lett.*, vol. 24, pp. 1490–1492, 1999.

[16] R. P. Mildren, H. M. Pask, H. Ogilvy, and J. A. Piper, "Discretely tunable, all-solid-state laser in the green, yellow, and red," *Opt. Lett.*, vol. 30, pp. 1500–1502, 2005.

[17] T. T. Basiev and R. C. Powell, "Solid-state Raman lasers," in *Handbook of Laser Technology and Applications*, C. E. Webb *et al.*, Ed. London, U.K.: Inst. Phys., 2003, ch. B1.7, pp. 469–497.

[18] H. M. Pask, "The design and operation of solid-state Raman lasers," *Progress Quantum Electron.*, vol. 27, pp. 1–56, 2003.

[19] P. Cerny, H. Jelinkova, P. G. Zverev, and T. T. Basiev, "Solid state lasers with Raman frequency conversion," *Progress Quantum Electron.*, vol. 28, pp. 113–143, 2004.

[20] R. W. Boyd, *Nonlinear Optics*. San Diego, CA: Academic, 1992.

[21] G. Eckhardt, "Selection of Raman laser materials," *IEEE J. Quantum Electron.*, vol. QE-2, no. 1, pp. 1–8, Jan. 1966.

[22] R. C. Powell, *Physics of Solid-State Laser Materials*. New York: Springer, 1998.

[23] T. T. Basiev, A. A. Sobol, P. G. Zverev, L. I. Ivleva, V. V. Osiko, and R. C. Powell, "Raman spectroscopy of crystals for stimulated Raman scattering," *Opt. Mater.*, vol. 11, pp. 307–314, 1999.

[24] T. T. Basiev, A. A. Sobol, Y. K. Voronko, and P. G. Zverev, "Spontaneous Raman spectroscopy of tungstate and molybdate crystals for Raman lasers," *Opt. Mater.*, vol. 15, pp. 205–216, 2000.

[25] A. A. Kaminskii, *Crystalline Lasers: Physical Processes and Operating Schemes*. Boca Raton, FL: CRC Press, 1996.

[26] A. A Kaminskii, H. J. Eichler, K. Euda, N. V. Klassen, B. S. Redkijn, L. E. Li, J. Findeisen, D. Jaque, J. Garcie Sole, J. Fernandez, and R. Balda, "Properties of $Nd3^+$-doped and undoped tetragonal $PbWO_4$, $NaY(WO_4)_2$, $CaWO_4$, and undoped monoclinic $ZnWO_4$ and $CdWO_4$ as laser-active and stimulated Raman-scattering active crystals," *Appl. Opt.*, vol. 38, pp. 4533–4547, 1999.

[27] A. A. Kaminskii, K. Ueda, H. J. Eichler, Y. Kuwano, H. Kouta, S. N. Bagaev, T. H. Chyba, J. C. Barnes, G. M. A. Gad, T. Murai, and J. Lu, "Tetragonal vanadates YVO_4 and $GdVO_4$—new efficient $\chi^{(3)}$-materials for Raman lasers," *Opt. Commun.*, vol. 194, pp. 201–206, 2001.

[28] H. M. Pask and J. A. Piper, "Diode-pumped $LiIO_3$ intracavity Raman lasers," *IEEE J. Quantum Electron.*, vol. 36, no. 8, pp. 949–955, Aug. 2000.

[29] T. T. Basiev, A. A. Sobol, P. G. Zverev, V. V. Osiko, and R. C. Powell, "Comparative spontaneous Raman spectroscopy of crystals for Raman lasers," *Appl. Opt.*, vol. 38, pp. 594–598, 1999.

[30] P. G. Zverev, T. T. Basiev, A. A. Sobol, V. V. Skornyakov, L. I. Ivleva, N. M. Polozkov, and V. V. Osiko, "Stimulated Raman scattering in alkaline-earth tungstate crystal," *Quantum. Electron.*, vol. 30, pp. 55–59, 2000.

[31] T. T. Basiev, S. V. Vassilev, M. E. Doroshenko, and V. V. Osiko, "Laser and self-Raman-laser oscillations of $PbMoO_4$:Nd^{3+} crystal under laser diode pumping," *Opt. Lett.*, vol. 31, pp. 65–67, 2006.

[32] P. G. Zverev, A. Y. Karasik, A. A. Sobol, D. S. Chunaev, T. T. Basiev, A. I. Zagumennyi, Y. D. Zavartsev, S. A. Kutovoi, V. V. Osiko, and I. A. Shcherbakov, "Stimulated Raman scattering of picosecond pulses in $GdVO_4$ and YVO_4 crystals," presented at the Tech. Dig. Adv. Solid State Photon. Conf., OSA, Washington, DC, 2004, Paper TuB10.

[33] I. V. Mochalov, "Laser and nonlinear properties of the potassium gadolinium tungstate laser crystal $KGd(WO_4)_2$ (KGW:Nd)," *Opt. Eng.*, vol. 36, no. 6, pp. 1660–1669, 1997.

[34] S. Biswal, S. P. O'Connor, and S. R. Bowman, "Thermo-optical parameters measured in ytterbium-doped- gadolinium tungstate," *Appl. Opt.*, vol. 44, pp. 3093–3097, 2005.

[35] M. Revermann, H. M. Pask, J. L. Blows, and T. Omatsu, "Thermal lensing measurements in an intracavity $LiIO_3$ Raman laser," presented at the Tech. Dig. Adv. Solid State Photon. Conf., OSA, Washington, DC, 2000, Paper ME13.

[36] H. M. Pask, J. L. Blows, J. A. Piper, and T. Omatsu, "Thermal lensing in a barium nitrate Raman laser," *OSA Trends Opt. Photon.: Adv. Solid State Lasers*, vol. 50, pp. 441–444, 2001.

[37] P. Dekker, H. M. Pask, and J. A. Piper, "All-solid-state 704 mW continuous-wave yellow source based on an intracavity, frequency-doubled crystalline Raman laser," vol. 32, pp. 1114–1116, 2007.

[38] P. Cerny and H. Jelinkova, "Near-quantum-limit efficiency of picosecond stimulated Raman scattering in $BaWO_4$ crystal," *Opt. Lett.*, vol. 27, pp. 360–362, 2002.

[39] T. T. Basiev, M. E. Doroshenko, V. V. Osiko, S. E. Sverchkov, and B. I. Galagan, "New mid IR (1.5–2.2 μm) Raman lasers based on barium tungstate and barium nitrate crystals," *Laser Phys. Lett.*, vol. 2, pp. 237–238, 2005.

[40] T. T. Basiev, M. N. Basieva, M. E. Doroshenko, V. V. Fedorov, V. V. Osiko, and S. B. Mirov, "Stimulated Raman scattering in the mid IR range 2.31–2.75–3.7 μm in a $BaWO_4$ crystal under 1.9 and 1.56 μm pumping," presented at the Tech. Dig. Adv. Solid State Photon. Conf., OSA, Washington, DC, 2006, Paper MB10.

[41] P. G. Zverev, T. T. Basiev, and A. M. Prokhorov, "Stimulated Raman scattering of laser radiation in Raman crystals," *Opt. Mater.*, vol. 11, pp. 335–352, 1999.

[42] C. He and T. H. Chyba, "Solid-state barium nitrate Raman laser in the visible region," *Opt. Commun.*, vol. 135, pp. 273–278, 1997.

[43] N. Takei, S. Suzuki, and F. Kannari, "20-Hz operation of an eye-safe cascade Raman laser with a $Ba(NO_3)_2$ crystal," *Appl. Phys.*, vol. B74, pp. 521–527, 2002.

[44] H. M. Pask, S. Myers, J. A. Piper, J. Richards, and T. Mckay, "High average power, all-solid-state external resonator Raman laser," *Opt. Lett.*, vol. 28, pp. 435–437, 2003.

[45] V. V. Ermolenko, V. A. Lisinetskii, Y. I. Mishkel, A. S. Grabchikov, A. P. Chaikovskii, and V. A. Orlich, "A radiation source based on solid-state Raman laser for diagnosing tropospheric ozone," *J. Opt. Technol.*, vol. 72, pp. 32–36, 2005.

[46] T. T. Basiev, Y. K. Danileiko, M. E. Doroshenko, V. V. Osiko, A. V. Fedin, A. V. Gavrilov, and S. N. Smetanin, "Powerful $BaWO_4$ Raman laser pumped by self-phase-conjugated Nd:YAG and Nd:GGG lasers," presented at the Tech. Dig. Adv. Solid State Photon. Conf., OSA, Washington, DC, 2004, Paper TuB11.

[47] R. P. Mildren, M. Convery, H. M. Pask, J. A Piper, and T. Mckay, "Efficient, all-solid-state, Raman laser in the yellow, orange and red," *Opt. Exp.*, vol. 12, pp. 85–790, 2004.

[48] R. P. Mildren, H. M. Pask, and J. A. Piper, "High-efficiency Raman converter generating 1.5 W of red-orange output," presented at the Tech. Dig. Adv. Solid State Photon. Conf., OSA, Washington, DC, 2006, Paper TuB10, Paper MC3.

[49] R. P. Mildren, H. Ogilvy, and J. A. Piper, "Solid-state Raman laser generating discretely tunable ultraviolet output at wavelengths 266–320 nm," Opt. Lett., vol. 32, pp. 814–816, 2007.

[50] S. Ding, X. Zhang, Q. Wang, F. Su, S. Li, S. Fan, J. Chang, S. Zhang, S. Wang, and Y. Liu, "Theoretical and experimental reearch on the multi-frequency Raman converter with $KGd(WO_4)_2$ crystal," *Opt. Exp.*, vol. 13, pp. 10120–10128, 2005.

[51] J. T. Murray, W. L. Austin, and R. C. Powell, "End-pumped intracavity solid-state Raman laser," in *Advanced Solid State Lasers,* (OSA Trends in Optics and Photonics Series vol. 19), W. Bosenberg and M. Fejer, Eds. Washington, DC: OSA, 1998, Paper IL11.

[52] H. M. Pask and J. A. Piper, "Practical 580 nm source based on frequency-doubling of an intracavity-Raman-shifted Nd:YAG laser," *Opt. Commun.*, vol. 148, pp. 285–288, 1998.

[53] A. S. Grabtchikov, A. N. Kuzmin, V. A. Lisinetskii, V. A. Orlovitch, G. I. Ryabtsev, and A. A. Demidovich, "All solid-state diode-pumped Raman laser with self-frequency conversion," *Appl. Phys. Lett.*, vol. 75, pp. 3742–3744, 1999.

[54] A. A. Lagatsky, A. Abdolvand, and N. V. Kuleshov, "Passive *Q* switching and self-frequency Raman conversion in a diode-pumped Yb:$KGd(WO_4)_2$ laser," *Opt. Lett.*, vol. 25, pp. 616–618, 2000.

[55] J. Findeisen, H. J. Eichler, and P. Peuser, "Self-stimulating, transversally diode-pumped Nd^{3+}:$KGd(WO_4)_2$ Raman laser," *Opt. Commun.*, vol. 181, pp. 129–133, 2000.

[56] W. Chen, Y. Inagawa, T. Omatsu, M. Tateda, N. Takeuchi, and Y. Usuki, "Diode-pumped, self-stimulating, passively Q-switched Nd^{3+}:$PbWO_4$ Raman laser," *Opt. Commun.*, vol. 194, pp. 401–407, 2001.

[57] J. Simons, H. M. Pask, P. Dekker, and J. A. Piper, "Compact diode-pumped 598-nm laser source," in *Solid State Lasers XI, Proceedings of SPIE*, vol. 4630, E. Scheps, Ed. Bellingham, WA: SPIE, 2002, pp. 57–64.

[58] P. Cerny, W. Zendzian, J. Jabczynski, H. Jelinkova, J. Sulc, and K. Kopczynski, "Efficient diode-pumped passively *Q*-switched Raman laser based on barium tungstate crystal," *Opt. Commun.*, vol. 209, pp. 403–409, 2002.

[59] A. A. Demidovich, P. A. Apanasevich, L. E. Batay, A. S. Grabtchikov, A. N. Kuzmin, V. A. Lisinetskii, V. A. Orlovich, O. V. Kuzmin, V. L. Hait, W. Kiefer, and M. B. Danaiov, "Sub-nanosecond microchip laser with intracavity Raman conversion," *Appl. Phys. B*, vol. 76, pp. 509–514, 2003.

[60] H. Ogilvy, H. M. Pask, and J. A. Piper, "All-solid-state, multi-kilohertz, 1.5 mm intracavity Raman aser based on Nd:YVO_4 and $KGd(WO_4)_2$," presented at the OSA Adv. Solid State Photon., Santa Fe, NM, 2004, Paper TuB12.

[61] A. A. Demidovich, L. E. Batay, A. S. Grabtchikov, V. A. Lisinetskii, V. A. Orlovich, and A. N. Kuzmin, "Self Raman conversion in YVO_4:Nd microchip laser," presented at the Tech. Dig. Adv. Solid State Photon. Conf., OSA, Washington, DC, 2004, Paper TuB9.

[62] Y. F. Chen, "High-power diode-pumped actively Q-switched Nd:YVO_4 self-Raman laser: Influence of dopant concentration," *Opt. Lett.*, vol. 29, pp. 1915–1917, 2004.

[63] Y. F. Chen, "Compact efficient all-solid-state eye-safe laser with self-frequency Raman conversion in a Nd:YVO_4 laser," *Opt. Lett.*, vol. 29, pp. 2172–2174, 2004.

[64] Y. F. Chen, "Compact efficient self-frequency Raman conversion in diode-pumped passively *Q*-switched Nd:$GdVO_4$ laser," *Appl. Phys. B*, vol. 78, pp. 685–687, 2004.

[65] Y. F. Chen, K. W. Su, H. J. Zhang, J. Y. Wang, and M. H. Jiang, "Efficient diode-pumped actively Q-switched Nd:YAG/$BaWO_4$ intracavity Raman laser," *Opt. Lett.*, vol. 30, pp. 3335–3337, 2005.

[66] J. Liu, U. Griebner, V. Petrov, H. Zhang, J. Zhang, and J. Wang, "Efficient continuous-wave and *Q*-switched operation of a diode-pumped Yb:$KLu(WO_4)_2$ laser with self-Raman conversion," *Opt. Lett.*, vol. 30, pp. 2427–2429, 2005.

[67] T. T. Basiev, S. V. Vassiliev, M. E. Doroshenko, V. V. Osiko, V. M. Puzikov, and M. B. Kosmyna, "Laser and self-Raman-laser oscillations of $PbMoO_4$:Nd^{3+} crystal under laser diode pumping," *Opt. Lett.*, vol. 31, pp. 65–67, 2006.

[68] J. Sulic, H. Jelinkova, M. E. Doroshenko, T. T. Basiev, L. I. Ivleva, V. V. Osiko, and P. G. Zverev, "Nd:$BaWO_4$ Raman laser," presented at the Tech. Dig. Adv. Solid State Photon. Conf., OSA, Washington, DC, 2006, Paper MB8.

[69] K. Maloney, D. Hwang, A. L. Oien, G. T. Bennett, M. Kukla, K. Burgio, and C. Anderson, "Compact short pulse eyesafe solid state Raman laser," presented at the Tech. Dig. Adv. Solid State Photon. Conf., OSA, Washington, DC, 2006, Paper MC2.

[70] Y. B. Band, J. R. Ackerhalt, J. S. Krasinski, and D. F. Heller, "Intracavity Raman lasers," *IEEE J. Quantum Electron.*, vol. 25, no. 2, pp. 208–132, Feb. 1989.

[71] J. T. Murray, P. T. Guerreio, L. K. Calmes, R. C. Powell, N. Peyghambarian, and W. L. Austin, "Pulse instabilities and chaos in intracavity Raman lasers," *OSA Trends Opt. Photon.: Adv. Solid State Lasers*, vol. 1, pp. 560–564, 1996.

[72] J. T. Murray, W. L. Austin, and R. C. Powell, "Intracavity Raman conversion and Raman beam cleanup," *Opt. Mater.*, vol. 11, pp. 353–371, 1999.

[73] R. P. Mildren, H. M. Pask, and J. A. Piper, "Raman lasers offer power and versatility," *Photon. Spectra*, vol. 39, pp. 52–59, 2005.

[74] H. M. Pask and J. A. Piper, "Design and operation of an efficient 1.4 W diode pumped Raman laser at 578 nm," *OSA Trends Opt. Photon.: Adv. Solid-State Lasers*, vol. 68, pp. 483–485, 2002.

[75] A. S. Grabitchikov, V. A. Linsinetskii, V. A. Orlovich, M. Scmitt, R. Maksimenka, and W. Kiefer, "Multimode pumped continuous-wave solid-sate Raman laser," *Opt. Lett.*, vol. 29, pp. 2524–2526, 2004.

[76] A. A. Demidovich, A. S. Grabtchikov, V. A. Linsinetskii, V. N. Burakevich, V. A. Orlovich, and W. Kiefer, "Continuous-wave Raman generation in a diode-pumped Nd^{3+}:$KGd(WO_4)_2$ laser," *Opt. Lett.*, vol. 30, pp. 1701–1703, 2005.

[77] V. A. Orlovich, V. N. Burakevich, A. S. Grabtchikov, V. A. Linsinetskii, A. A. Demidovich, H. J. Eichler, and P. Y. Turpin, "Continuous-wave intracavity Raman generation in $PbWO_4$ crystal in the Nd:YVO_4 laser," *Laser Phys. Lett.*, vol. 3, pp. 71–73, 2006.

[78] H. M. Pask, "Continuous-wave, all-solid-state intracavity Raman laser," *Opt. Lett.*, vol. 30, pp. 2454–2456, 2005.

[79] T. Omatsu, A. Lee, P. Dekker, H. M. Pask, and J. A. Piper, "Compact continuous-wave yellow laser based on a self-stimulating Raman Nd:YVO_4 laser," presented at the OSA Adv. Solid State Photon. Conf., Vancouver, BC, Canada, Feb. 2007, Paper WB19.

[80] H. Rong *et al.*, "An all-silicon Raman laser," *Nature*, vol. 433, pp. 725–728, 2005.

[81] H. Rong, Y-H Kuo, S. Xu, A. S. Liu, R. Jones, and M. Panicca, "Monolithic integrated Raman silicon laser," *Opt. Exp.*, vol. 14, pp. 6705–6712, 2006.

James A. Piper received the B.Sc. and Ph.D. degrees in physics from the University of Otago, Dunedin, New Zealand, in 1968 and 1971, respectively.

He was a Postdoctoral Researcher in the field of gas lasers at Clarendon Laboratory, Oxford University, Oxford, U.K. He joined as a Faculty Member at Macquarie University, Sydney, Australia, and was appointed as the Chair in the Department of Physics in 1984.

His research has been concerned with copper vapor lasers, dye lasers, excimer lasers, all-solid-state lasers, including self-frequency-doubling lasers and intracavity crystalline Raman lasers, and applications in microfabrication and biomedicine. He is currently the Deputy Vice Chancellor (Research) at Macquaric University.

Dr. Piper is a Fellow of the Optical Society of America. He was awarded the 2006 Carnegie Centenary Professorship hosted by Heriot-Watt University, Edinburgh, U.K.

Helen M. Pask received the B.Sc. and Ph.D. degrees in physics from Macquarie University, Sydney, Australia, in 1987 and 1992, respectively.

She was a Postdoctoral Researcher in the field of fiber lasers at the Unversity of Southampton, Southampton, U.K. In 1995, she joined the Macquarie University, Sydney, Australia, where she is currently an Innovation Fellow at the Centre for Lasers and Applications, Department of Physics. Her current research interests include fiber lasers, crystalline Raman lasers, and visible solid-state lasers.